Materials for life sciences

Non-enzymatic potentiometric malathion sensing over chitosan-grafted polyaniline hybrid electrode

Chandra Shekhar Kushwaha[1] and S. K. Shukla[1,*]

[1] *Department of Polymer Science, Bhaskaracharya College of Applied Sciences, University of Delhi, Delhi 110075, India*

ABSTRACT

Non-enzymatic electrochemical malathion sensing has been demonstrated over chitosan-grafted polyaniline (CHIT-g-PANI)-based electrode. Structural, morphological, and physical properties of electrode were investigated by Fourier transform infrared (FTIR) spectrometer, X-ray diffraction (XRD), scanning electron microscope (SEM), thermal analysis (TGA), and other relevant ASTM methods. The obtained result suggests the formation of porous hybrid matrix with better free complexing group, electrical conductivity, and thermal stability due to rearrangement of molecular structure and crystallinity. Further, CHIT-g-PANI-based electrode was used for potentiometric sensing of malathion (MLT) in tomato juice by monitoring induced potential due to surface interaction between MLT and CHIT-g-PANI-based electrode. The observed sensing parameters are sensing range 62.5 to 2.0 μM, sensitivity 2.26 mV μM^{-1} cm^{-2}, limit of detection 3.8 μM, response time 8.0 min, and recovery time 30 s. On the basis observed results a charge transferring, weak surface complexation-based sensing mechanism was proposed in fruits and vegetables in competitive and cost-effective manner.

Introduction

Diethyl 2-[(dimethoxy-phosphorothioyl) sulfanyl] butanedioate or MLT is a widely used in pesticides in agriculture as well as to control the pests, insects, and microbes in different government programs. MLT is a chemically stable and highly harmful organic compound for the aquatic organisms, vertebrates as well as human beings by intervening the nervous systems [1, 2]. It is reported that excess use of MLT is contaminating the groundwater, food, vegetable, and other agricultural products. These contaminated products are creating serious negative impact on health of humans, animals, and vegetations [3, 4]. The continuous exposure of MLT causes nausea, chest tightness, headache, convulsions, long-term illness, and suppress the immune system [5, 6]. Thus, sensing and monitoring of MLT is an important need for human health and environmental poisoning.

The techniques used for quantification of MLT are gas chromatography, high-performance liquid chromatography [7, 8], colorimetry [9], electrophoresis, and Raman spectroscopy [10]. These techniques are sensitive, reliable, and efficient, but they have several

Address correspondence to E-mail: sarojshukla2003@yahoo.co.in

drawbacks like bulky size instruments, complicated operational and pretreatment process, high cost, and long analysis times. Thus, several research groups are involved in developments of different type of MLT sensor using several advanced hybrid materials. Generally, a sensor works on the basis of monitoring the induced optical, electrical, and mechanical signal generated after interaction of MLT on a sensing substrate. Among different types of sensor, electrochemical sensors are more reliable, reproducible, and commercialized. Most of the electrochemical sensors are comprised of acetylcholinesterase (AChE), an enzyme for selective oxidation. These sensors are very sensitive and accurate for detection of MLT in different samples. However, they are not useful for long-term sensing due to the poor chemical and physical stability of the enzyme. The activity of enzyme is also lost due to contamination of heavy metals and pesticide [11, 12].

Thus, the development of non-enzymatic sensors is important for the detection of MLT in harsh conditions. Representative MLT sensors are listed in Table 1 along with properties. In non-enzymatic electrochemical sensor, the change in electrochemical signal is monitored after the interaction of malathion on surface of sensing electrode. These sensors bear several disadvantages like poor selectivity and also sensitivity. The several composites with biocompatibility and catalytic properties are explored with limited feature. In this regard, we have developed a state-optimized electroactive chitosan-grafted polyaniline (CHIT-g-PANI) hybrid matrix by in situ polymerization and composite formation techniques. This hybrid matrix exhibits good interactive sites, conductivity, good stability, film-forming ability, and biocompatibility to provide promising electrochemical response toward residual MLT present in tomato available in India.

Experimental

Chemicals

Chitosan (CHIT, > 75% deacetylated, Mw 120−150 K), aniline (99.5%), ammonium persulfate (APS) (99.5%), and MLT were purchased from Sigma-Aldrich and used without any further purification. The other used supplementary chemicals were of analytical grades, and solutions were prepared with Milli-Q water throughout investigation.

Preparation of chitosan-*grafted*-polyaniline

Initially, solution of CHIT was prepared by mixing of 1.0 g CHIT flakes in 25 mL acetic acid/water mixture (25% v/v, pH ∼ 4). The solution was stirred magnetically for 2 h at room temperature, and a flake-free clear solution was obtained. The solution was stored at 4 °C in refrigerator for further use. Aniline solution was also prepared by mixing 5 mL aniline in 20 mL 0.1 M aqueous HCl solution after stirring it magnetically for 1 h at room temperature. Further, to prepare composite 10 mL of flake-free CHIT solution and 6.5 mL aniline solution were mixed in 250-mL beaker after constant stirring on a magnetic stirrer. The resultant solution was polymerized after drop by drop adding 50 mL aqueous solution of 0.1 M ammonium persulfate after maintaining the temperature at 0–5 °C on an ice-bath. After 30 min, a greenish-blue color precipitate was obtained, which was allowed to settle down over night. Finally, obtained precipitate was filtered and washed by deionized water and then dried in vacuum oven at 60 °C for 24 h. The dried copolymer was further extracted successively with m-cresol and dimethyl sulfoxide in a soxhlet apparatus for 36 h, in order to purify the copolymer.

Preparation of electrode

Five hundred milligrams of CHIT-g-PANI was dispersed in 20 mL NMP in a beaker. Thus obtained solution was casted on a corning glass slide with dimension 1 cm × 0.5 cm × 0.1 cm and using a spin coater working a 500 rpm. The obtained film was further dried in a vacuum oven and used as a electrode.

Instrumentation

The spectroscopic analysis of obtained CHIT-g-PANI matrix was carried out using a Perkin-Elmer (RK-1310) FTIR spectrometer. The spectra were recorded in KBr phase after accumulation of 16 scan with resolution of 2 cm^{-1} in the range of 4000 to 400 cm^{-1}. The particle phase, size, and structure were studied using X-ray powder diffraction pattern on the Rigaku

**Table 1** Representative MLT sensors with sensing parameters

S. No.	Materials	Transducer	Enzymatic or non-enzymatic	Detection range	Sensitivity	Remarks	Ref.
1	PANI-ES/ SWCNTs graphite	Electrochemical (DPV)	Non-enzymatic	2.0×10^{-7} M to 14.0×10^{-7} M	7.22 mA/ μM	Detection limit 2.0×10^{-7} M	[13]
2	AuNPs-CS-IL/ PGE	Voltammetric (SWV)	Non-enzymatic	Two linear range 0.89–5.94 nM and 5.94–44.6 nM	–	Detection limit 0.68 nM	[14]
3	CuO NWs–SWCNTs	Electrochemical (DPV)	Non-enzymatic	0 to 120 nM	–	Detection limit 0.1 ppb (0.3 nM),	[15]
4	CuO nanostructure modified GCEs	Electrochemical (DPV)	Non-enzymatic	1 nM–12 nM	1089.85 μA nM^{-1} cm^{-2}	Detection of limit 0.1 nM	[16]
5	Eggshell membrane (ESM)	Optical	Enzymatic	0.1–50 ng/mL	–	Detection limit 0.1 ng/mL within 30 min	[17]
6	PMAA-AuNPs-APTAMER	Optical	Enzymatic	3.3–33.3 μg/mL^{-1}	–	Detection limit 3.3 μg-mL^{-1}	[18]
7	dsCT-DNA-PPy-PVS	Electrochemical (CV)	Enzymatic	0.17–5.0 ppm	–	Detection 0.17 ppm and response time is 30 s	[19]
8	CHIT-g-PANI	Potentiometric	Non-enzymatic	2.0–62.5 μM	2.26 mV μM^{-1} cm^{-2}	Detection limit 3.8 μM and response time is 8.0 min.	This work

Rotaflex, RAD/Max-200B X-ray diffractometer using CuKα (λ = 1.5405 Å) radiation at a scanning rate of 2° per min. Further, surface morphology was examined by JSM-6100 model SEM, operated at working voltage of 30 kV. Thermal gravimetric analysis was recorded on Linesis, (TA-Evaluation, V-2-3-1) thermogravimetric instrument, at heating rate of 10 °C per min and 100 mL per minute nitrogen gas flow rate.

Fabrication of sensing device

The complete setup is shown in Fig. 1. Initially, two cylindrical glass chamber A and B with 100 mL capacity were taken, which were connected with glass tube having diameter of 2 mm and length 2.0 cm using nafion membrane in between. The chamber A was used as a reference electrode, while chamber B for sensing of MLT from the developed electrode. The induced potential was measured between the sensing and reference electrode [21]. The potentiometric sensitivity was measured in a freshly prepared malathion solution filled in chamber B at
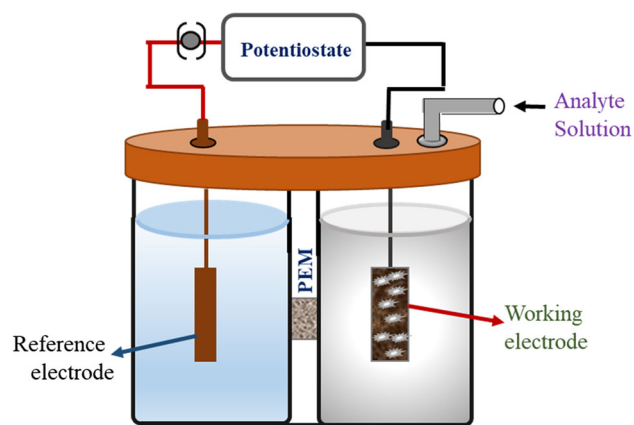
Figure 1 Schematic diagram of potentiometric sensor.

different concentration (2.0 µM to 62.5 µM) at 20–25 °C after maintaining the pH by addition suitable buffer. Initially, solutions were stirred for 10 s, and potential was recorded after stabilization of the potential. A stock solution of MLT in acetone was prepared. The stock solution was further diluted by 0.1 M phosphate buffer (pH = 7) to obtained solutions of MLT with a concentration range of 10^{-6} M. The detection of MLT was carried out by measuring potential developed during electrochemical oxidation of MLT of concentration 2.0 µM to 62.5 µM.

The sensing was also made for real sample. In this regard, tomato was procured from the mother dairy, Delhi. It was cleaned with distilled water and chopped into small pieces. The 100 gm of chopped tomato was grilled in electric mixer for 10 min at 500 rpm to obtained pest followed by centrifuge for 15 min at 1000 rpm collection of the supernatant for analysis. The other parameters were also recorded using a similar setup after coupling requisite parameters. The used electrode was washed with acetone by dipping for 1 min and then in double-distilled water for 2–3 min and then dried in hot air oven for 30 min to explore its reusability.

Electrical conductivity

Electrical conductivity of electrode was determined by plotting I–V curve. The voltages were applied with the help of 32-V Aplab regulated DC power supply, and respective current was measured using Scientech Digital Multimeter DM-97.

Physicomechanical properties

The physicomechanical properties, i.e., solvent content, thickness, swelling, and porosity of the bioelectrode, were estimated standard ASTM method as discussed in [20].

Solvent content and degree of swelling

Initially, a film of CHIT-g-PANI was cut in size of 1 cm × 1 cm with a surgical blade. The film was soaked in the 1 M aqueous solution of sodium chloride for 24 h. After then, it was taken out, blotted quickly with a Whatman filter paper to remove the surface adsorbed water, and then weighed immediately. Further, electrode was dried to a constant weight in vacuum oven over silica gel and

temperature 50 °C. The solvent uptake content (% total wet weight) is calculated using Eq. 1:

$$S = \frac{W_w - W_d}{W_w} \times 100 \qquad (1)$$

where W_w is the weight of wet film and W_d is the weight of dried film.

However, the degree of swelling of electrode was estimated by the difference between the average thickness of the wet film equilibrated with NaCl solution for 24 h and that of the dry film.

Porosity

Porosity (E) was calculated as the volume of solvent incorporated in the cavities present per unit electrode volume using Eq. 2:

$$E = \frac{W_s - W_d}{AL\delta_w} \qquad (2)$$

where W_s is soaked weight, W_d is dry weight, A is area, L is thickness of film, and δ_w is density of water.

Result and discussion

FTIR spectra

FTIR spectra of pure PANI and on CHIT-g-PANI are shown in Fig. 2 along with characteristics peaks in Table 2. The characteristic band of PANI for N=Q=N vibrations, aromatic C–N stretching, C=C, C=N of benzenoid and quinoid stretching are shifted to lower wavenumber in the CHIT-g-PANI. The lower shift in wavenumbers of composite copolymer indicates the grafting of chitosan with PANI.

The broad IR peak at 3432 cm^{-1} can be assigned to the stretching mode of N–H in PANI, which slightly shifted lower at 3427 in composite due to interaction of –OH and N–H of chitosan along with appearance of a peak at and 3424 cm^{-1}, while the intensity of broad peak quite reduced due to overlapping of O–H stretching of chitosan and N–H stretching of aniline groups at PANI. The appearance of a shoulder peak is indicating the generation of free group in hybrid matrix during grafting.

Another important observed change is the ratio of benzenoid and quinoid form due to grafting with CHIT from 0.166 to 0.4. Thus, FTIR spectra confirm the grafting, electrostatic forces, and the hydrogen
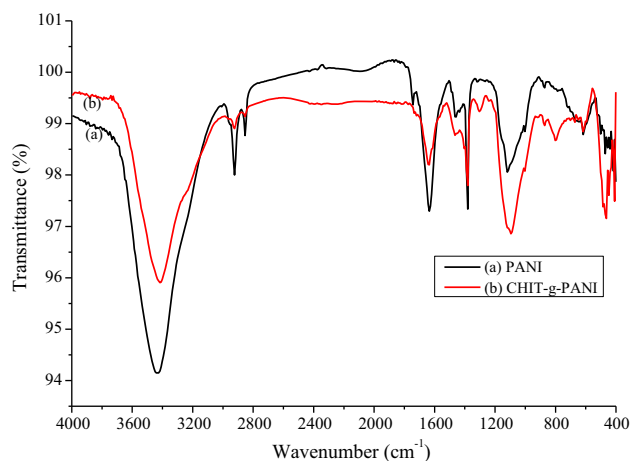
Figure 2 FTIR spectra of PANI and CHIT-g-PANI.

bonding between the moieties of chitosan and aniline [22]. The possible grafted structure of chitosan and PANI in composite is shown in Fig. 3.

XRD

Figure 4 shows X-ray diffraction pattern of PANI and CHIT-g-PANI copolymer. The characteristic peaks of PANI are present at 2θ value of 20.2 and 25.6° in its spectra due to 100 and 110 plane. However, XRD pattern of CHIT-g-PANI shows peaks at 19.8°, 25.2° due to PANI and at 29.4°, 37.6°, and 43.9° due to CHIT. The shifting from 20.2° to 19.8° and 25.6° to 25.3° reveals the formation of intercalated type CHIT-g-PANI hybrid matrix due to increase in interplanar spacing of PANI matrix due intercalation of CHIT molecules[23, 24]. The separation of matrix also supports the generation of free group in hybrid than its constituents. The intensity of peaks also shows some changes. It may be due to grafting of PANI with CHIT particles, which optimized the crystallinity in hybrid matrix.
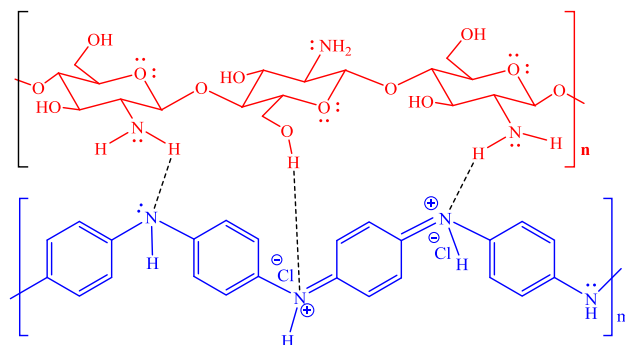

Figure 3 Schematic diagram of CHIT-g-PANI copolymer.

SEM

The surface morphology and particle size of PANI and CHIT-g-PANI copolymer were studied using SEM. The SEM image of PANI (Fig. 5a) indicates the formation homogenous morphology with spherical particles. However, Fig. 5b indicates the binary structure of CHIT-g-PANI composite, which contains the two types of particles for chitosan and PANI both.
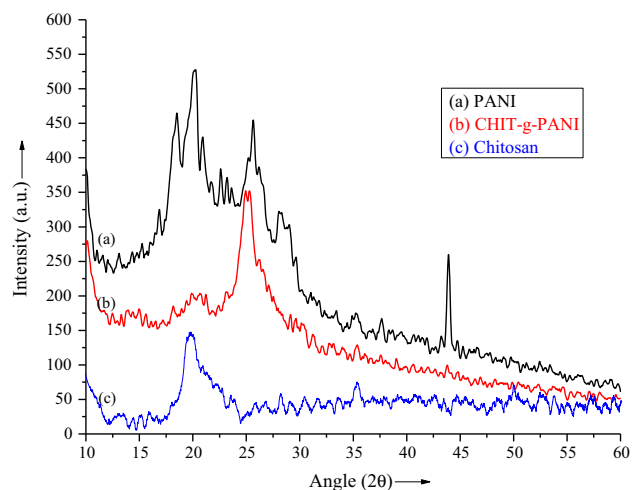

Figure 4 XRD pattern of PANI and CHIT-g-PANI composite.

Table 2 FTIR data and interpretation of peak

S. No.	PANI	CHIT-g-PANI	Assigned Group
1	809	794	p-disubstituted aromatic ring
2	1118	1095	N=Q=N vibrations
3	–	1295	Due to C–N stretching of chitosan
4	1380	1380	Aromatic C–N stretching
5	1457	1457	C=C, C=N stretching of benzenoid rings
6	1643	1635	C=C, C=N stretching of quinoid rings
7	2854–2923	2854–2923	C–H stretching of chitosan
8	3432 (br)	3427 (br)	N–H and O–H stretching of chitosan and PANI

Figure 5 SEM image of (**a**) PANI, **b** CHIT-g-PANI composite.
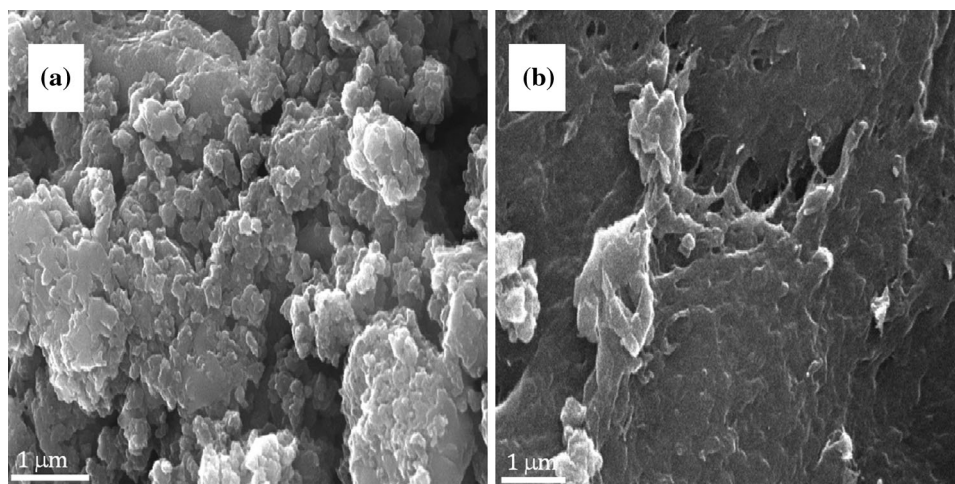
Conductivity measurement

The measured electrical conductivity of PANI and CHIT-g-PANI copolymer is given in Table 3. The result indicates that electrical conductivity of copolymers was approximately in the same order than pure PANI. However, the conductivity of copolymer slightly decreases due to the incorporation of non-conducting chitosan.

Thermal stability

TG curve of PANI and CHIT-g-PANI is shown in Fig. 6. The thermogram of PANI is indicating initial weight loss of 8–10% up to 120 °C due to the removal of moisture and adsorbed solvent. Further, a sharp decomposition of PANI proceeded with loss of 88% between 315 and 485 °C. However, CHIT-g-PANI indicates a weight loss in three steps first up to 150 °C, second between 180 and 305 °C, and last weight loss between 305 and 633 °C. The third step indicates the presence of binary matrix due to grafting of chitosan and PANI. The slow decomposition process of hybrid between 305 and 633 °C of CHIT-g-PANI was attributed to the formation binary matrix with intermolecular and intramolecular H-bonds.

Table 3 Electrical conductivity of composites

S. No	Materials	Conductivity (S cm^{-1})
1	PANI	4.19×10^{-5} S cm^{-1}
2	CHIT-g-PANI	2.10×10^{-6} S cm^{-1}

Malathion sensing

The potential variation with concentration of MLT is shown in Fig. 7. The graph is indicating a linear change in potential response in the range of 2.0 to 62.5 μM. The slope of potential curve of CHIT-g-PANI reveals the sensitivity as well as sensing response.

The observed sensing response of proposed sensor is 2.26 mV μM^{-1} cm^{-2}, which is much better than several earlier reported malathion sensors [Table 1]. Further, limit of detection (LOD) was calculated and found to be 3.8 μM. The change in potential of sensor was also recorded with time, and the graph is shown in Fig. 8.

It reveals that the potential of developed electrode continuously increases and 80% increase is found in 110 s and then becomes constant. Further, potential
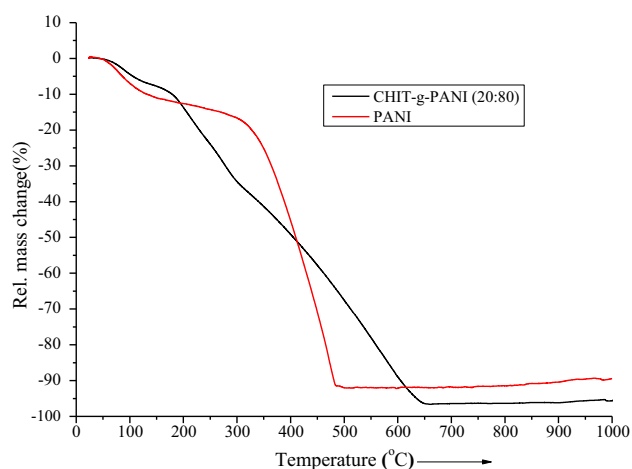

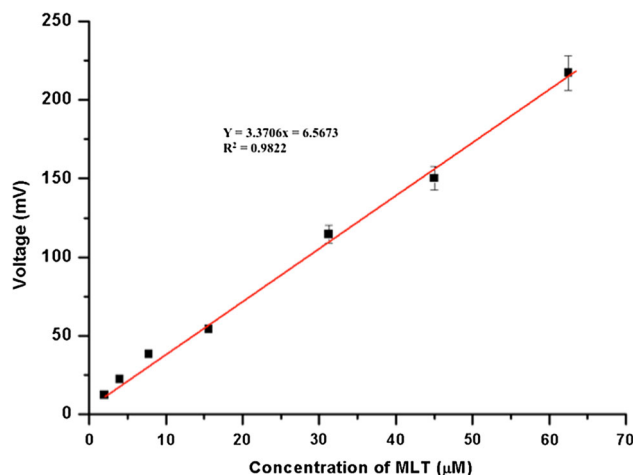**Figure 6** TG curve of PANI and CHIT-g-PANI analysis of composites.

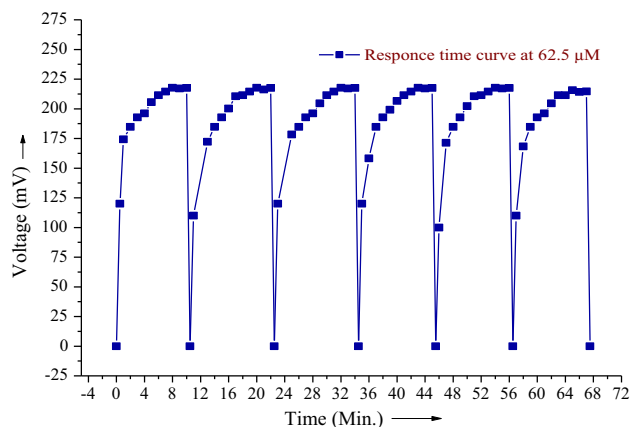**Figure 7** Potential variation on CHIT-g-PANI/ITO electrode with MLT.

Table 4 Residual MLT sensing in Indian tomato

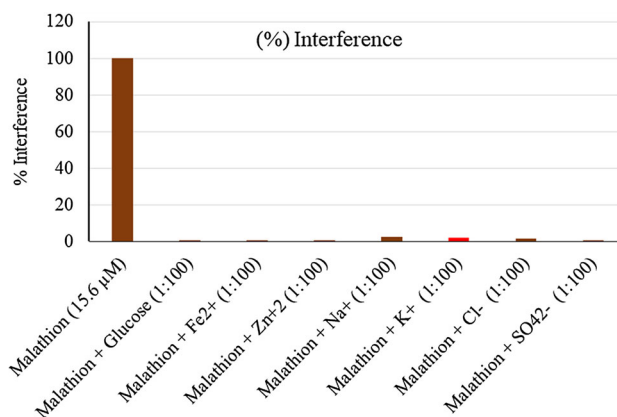| Sample No.	Spectroscopic methods (μM)	Developed method (μM)
1	52.2	52.8
2	38.3	38.0
3	42.5	41.3
4	35.6	37.3
5	26.5	27.1

Figure 9 Interference study of developed MLT sensor.

response was examined for 100-fold higher quantity of interferent than that of concentration of malathion. The results are given in Fig. 9, which reveals the negligible interference on the working electrode.

Figure 8 Potential variation on bioelectrode with time.

quickly regains its original value in 25 s regularly. Thus the response time and recovery time of sensor are 110 s and 25 s along with précised reproducibility.

Analysis of real samples

The developed sensors were also used for sensing of MLT in tomato samples for commercial application. The results are given in Table 4.

The results indicate the suitability of developed sensor in accordance with spectroscopic method.

Interference study

The interference of possible interfering substances on the determination of malathion was studied for 15.6 μM concentration of malathion. The electrode

Repeatability, reliability, and mechanism

This sensitivity of electrode was tested with time interval of 24 h for 45 days. The only drop of 3% sensing signal is found, which indicates the better usability than enzyme-immobilized electrode for a long time. The sensitivity of reused electrode was also tested and was found to be stable for 10 times. This indicates its reliability after satisfactory use due to nonsignificant change in signal of sensor. The sensing efficiency of electrode was decreased 2% after 50 times use.

The reported sensing mechanism of MLT is based on selective oxidation by either microbes, enzymes, or DNA. The oxidation generates electron after oxidation of MLT. However, in present case, IR spectra of electrode were recorded before and after MLT sensing to understand the sensing mechanism. The spectra are shown in Fig. 10, which indicates the presence of additional peaks at 515 along with
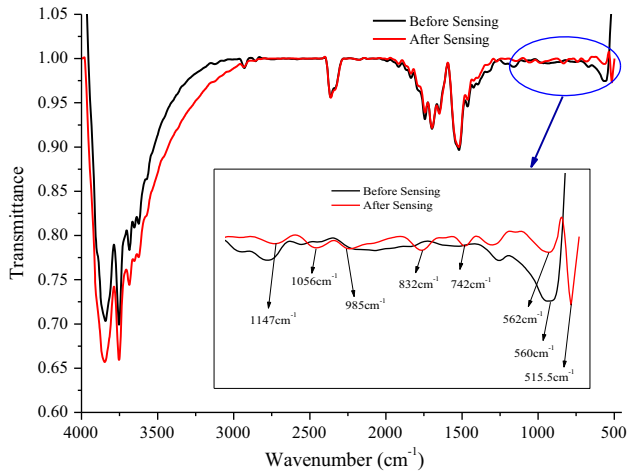
Figure 10 FTIR spectra of CHIT-g-PANI electrode before and after MLT sensing.

change in position of characteristic peaks due to the interaction between MLT on CHIT-g-PANI matrix. This change in spectra indicates that the formation of free group in hybrid with expanded hybrid matrix of electrode that supports the interaction with MLT [25].
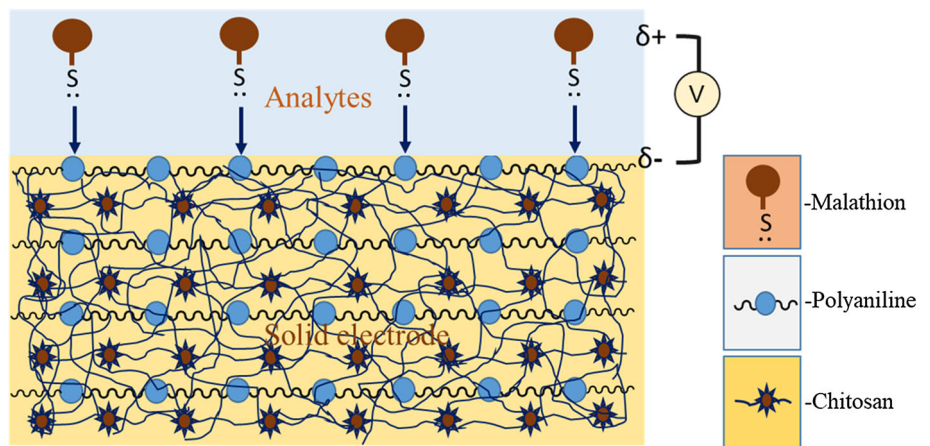
The formation of expanded matrix with free group is also responsible for improvement in physicomechanical properties. The observed properties are given in Table 5.

The above results indicate the formation of porous matrix and large adsorption capacity with interactive

sites. Thus, the sulfur atom of MLT interacts with electrode and partially transfers the electron to the CHIT-g-PANI. This partial shift of electron from MLT creates electron drift and induces potential for quantification of MLT. However, biocompatibility and large chain and porous nature of CHIT provide efficient conduction and adsorption. Furthermore, the biocompatible CHIT and porous nature of electrode support large adsorption capacity of MLT due to the formation of expanded matrix after grafting. A schematic presentation of sensing mechanism is shown in Fig. 11.

Conclusion and future outlook

An electrochemical malathion sensor-based CHIT-g-PANI copolymer has been fabricated by in situ method, and electrode was fabricated by spin coating method on ITO-coated glass. The electrochemical sensing showed a linear response to malathion concentrations ranging from 2.0 to 62.5 µM with sensitivity 2.26 mV µM^{-1} cm^{-2}, response time of 8 min, and long-term stability. These results indicate that the proposed electrode also has negligible interference effect and thus could be a promising option for the development of simple non-enzymatic electrochemical portable sensors in the future.

Table 5 Physico-mechanical properties of CHIT and CHIT-g-PANI

S. No	Composite materials	Solvent uptake (%)	Swelling (%)	Porosity
1	CHIT	51	39	0.0067
2	CHIT-g-PANI	59	48	0.0158

Figure 11 Illustration of sensing mechanism.

Acknowledgements

References

[1] Ahmed M, Rocha JBT, Mazzanti CM, Morsch ALB, Cargnelutti D, Corrêa M, Loro V, Morsch VM, Schetinger MRC (2007) Malathion, carbofuran and paraquat inhibit *Bungarus sindanus* (krait) venom acetylcholinesterase and human serum butyryl-cholinesterase in vitro. Ecotoxico 16(4):363–369

[2] Zhang Q, Jing Y, Shiue A, Chang CT, Ouyang T, Lin CF, Chang YM (2013) Photocatalytic degradation of malathion by TiO_2 and $Pt-TiO_2$ nanotube photo-catalyst and kinetic study. J Environ Sci Health B 48(8):686–692

[3] Madianos L, Skotadis E, Tsekenis G, Patsiouras L, Tsigkourakos M, Tsoukalas D (2018) Impedimetric nanoparticle aptasensor for selective and label free pesticide detection. Microelectron Eng 189:39–45

[4] Nsibande SA, Forbes PBC (2016) Fluorescence detection of pesticides using quantum dot materials–a review. Anal Chim Acta 945:9–22

[5] Raghu P, Reddy TM, Reddaiah K, Swamy BEK, Sreedhar M (2014) Acetylcholinesterase based biosensor for monitoring of malathion and acephate in food samples: a voltammetric study. Food Chem 142:188–196

[6] Aprea C, Strambi M, Novelli MT, Lunghini L, Bozzi N (2000) Biologic monitoring of exposure to organophosphorus pesticides in 195 Italian children. Environ Health Perspect 108(6):521–525

[7] Bavcon M, Trebše P, Zupančič-Kralj L (2003) Investigations of the determination and transformations of diazinon and malathion under environmental conditions using gas chromatography coupled with a flame ionization detector. Chemosphere 50:595–601

[8] Abu-Qare AW, Abou-Donia MB (2001) Simultaneous determination of malathion, permethrin, DEET (N, N-diethyl-m-toluamide), and their metabolites in rat plasma and urine using high performance liquid chromatography. J Pharm Biomed Anal 26:291–299

[9] Clark ER, Qazi IA (1979) Modified colorimetric method for the determination of malathion. Analyst 104:1129–1134

[10] Quintás G, Garrigues S, De La Guardia M (2004) FT-Raman spectrometry determination of Malathion in pesticide formulations. Talanta 63:345–350

[11] Li H, Wang Z, Wu B, Liu X, Xue Z, Lu X (2012) Rapid and sensitive detection of methyl-parathion pesticide with an electropolymerized, molecularly imprinted polymer capacitive sensor. Electrochim Acta 62:319–326

[12] Zhou JH, Deng CY, Si SH, Wang SE (2011) Zirconia electrodeposited on a self-assembled monolayer on a gold electrode for sensitive determination of parathion. Microchim Acta 172(1–2):207–215

[13] Ebrahim S, El-Raey R, Hefnawy A, Ibrahim H, Soliman M, Abdel-Fattah TM (2014) Electrochemical sensor based on polyaniline nanofibers/single wall carbon nanotubes composite for detection of malathion. Synth Met 190:13–19

[14] Bolat G, Abaci S (2018) Non-enzymatic electrochemical sensing of malathion pesticide in tomato and apple samples based on gold nanoparticles-chitosan-ionic liquid hybrid nanocomposite. Sensors 18(3):773. https://doi.org/10.3390/s18030773

[15] Huo D, Li Q, Zhang Y, Hou C, Lei Y (2014) A highly efficient organophosphorus pesticides sensor based on CuO nanowires–SWCNTs hybrid nanocomposite. Sens Actuators B: Chem 199:410–417

[16] Soomro RA, Hallam KR, Ibupoto ZH, Tahira A, Sherazi STH, Memon SS, Willander M (2016) Amino acid assisted growth of CuO nanostructures and their potential application in electrochemical sensing of organophosphate pesticide. Electrochim Acta 190:972–979

[17] Kaur N, Thakur H, Pathak S, Prabhakar N (2015) Acetylcholinesterase immobilized eggshell membrane-based optical biosensor for organophosphate detection. Int J Environ Anal Chem 95(12):1134–1147

[18] Barahona F, Bardliving CL, Phifer A, Bruno JG, Batt CA (2013) An aptasensor based on polymer-gold nanoparticle composite microspheres for the detection of malathion using surface-enhanced Raman spectroscopy. Ind Biotechnol 9(1):42–50

[19] Prabhakar N, Arora K, Singh SP, Pandey MK, Singh H, Malhotra BD (2007) Polypyrrole-polyvinyl sulphonate film based disposable nucleic acid biosensor. Anal Chim Acta 589(1):6–13

[20] Gupta AP, Agrawal H, Shukla SK, Bhardwaj R (2004) Studies on PVC based chelating inorganic ion exchange resin membrane sensor for neodymium(III) ion. J Ind Chem Tech 11:500–503

[21] Shukla SK, Deshpande SR, Shukla SK, Tiwari A (2012) Fabrication of a tunable glucose biosensor based on zinc oxide/chitosan-graft-poly(vinyl-alcohol)core-shell nanocomposite. Talanta 99:283–287

[22] Yavuz AG, Uygun A, Bhethanabotla VR (2009) Substituted polyaniline/chitosan composites: synthesis and characterization. Carbohyd Polym 75(3):448–453

[23] Shukla SK, Tiwari A (2011) Synthesis of chemical responsive chitosan–grafted-polyaniline bio-composite. Adv Mater Res 306–307:82–86

[24] Kushwaha CS, Singh P, Shukla SK, Dubey GC (2018) Electrochemical urea sensing over polyaniline grafted chitosan copolymer. Mater Today: Proc 5(7):15253–15260

[25] Kalantary RR, Azari A, Esrafili A, Yaghmaeian K, Moradi M, Sharafi K (2016) The survey of Malathion removal using magnetic graphene oxide nanocomposite as a novel adsorbent: thermodynamics, isotherms, and kinetic study. Desalination Water Treat 57(58):28460–28473